Chaos, Solitons & Fractals 45 (2012) 1092–1099

Contents lists available at SciVerse ScienceDirect

Chaos, Solitons & Fractals

Nonlinear Science, and Nonequilibrium and Complex Phenomena

journal homepage: www.elsevier.com/locate/chaos

Nonlinear dynamic analysis of 2-DOF nonlinear vibration isolation floating raft systems with feedback control

Yingli Li, Daolin Xu *, Yiming Fu, Jiaxi Zhou

State Key Lab. of Advanced Technology of Design and Manufacturing for Vehicle Body and College of Mechanical and Vehicle Engineering, Hunan University, Changsha 410082, PR China

ARTICLE INFO

Article history:
Received 8 March 2012
Accepted 24 June 2012
Available online 20 July 2012

ABSTRACT

In this paper, the average method is adopted to analysis dynamic characteristics of nonlinear vibration isolation floating raft system with feedback control. The analytic results show that the purposes of reducing amplitude of oscillation and complicating the motion can be achieved by adjusting properly the system parameters, exciting frequency and control gain. The conclusions can provide some available evidences for the design and improvement of both the passive and active control of the vibration isolation systems. By altering the exciting frequency and control gain, complex motion of the system can be obtained. Numerical simulations show the system exhibits period vibration, double period vibration and quasi-period motion.

1. Introduction

There are many noise and vibration sources on-board an underwater vehicle whose amplitude and spectra feature must be controlled in order to provide the submarine with a stealth capability to perform many of its intended missions. To enhance the stealth capability, the submarine should minimise the acoustic noise that is broadcast into the water and prevent it from being detected by active sonar methods, where a sonar signal is broadcast from another platform and listens to the reflected signals. Besides, employing noise and vibration control technologies on-board a submarine is to minimise the exposure to personnel, provide a comfortable working environment thereby reducing fatigue of personnel, reduce the fatigue of machinery parts, resulting in an improvement in reliability and reduced maintenance costs. To achieve this goal, much effort has been dedicated to the vibration isolation of the submarine [1–5]. There is also a bunch of researchers working on the idea of chaotification of the system, to alter the frequency spectra feature of the vibration and improve the concealment capability of underwater vehicles [6–9]. Line spectra of noise radiated from machinery vibration of underwater vehicles signify dynamical characteristics of operating systems, usually employed as a means for identification of vehicles. By purposely operating a nonlinear vibration isolation system (VIS) on chaotic state, it is possible to convert harmonic machinery vibrations to chaotic motions. In this process, narrow-band line spectra of harmonic vibration noise can be converted onto broadband spectra of chaos. Because of the broadband nature of chaos, major part of vibration energy at the machinery excitation frequency could be through VIS scattered over a wide frequency domain, resulting in the reduction of intensity of line spectra. The vibration isolation performance of chaos-based nonlinear vibration isolators was found to be superior to that of traditional ones in the sense of line spectra reduction [10].

In general, if the vibration source can be minimised in the first place, then there is no need for ameliorative systems to fix problems. Some vibration control methods involve treating the transmission path, by using vibration isolators to prevent the vibration from reaching a receiver. In few cases it is possible to relocate the receiver to lessen the perceived issue. The usual control techniques involve

* Corresponding author.
E-mail addresses: dlxu001@gmail.com, dlxu@hnu.edu.cn (D. Xu).

0960-0779/$ - see front matter © 2012 Elsevier Ltd. All rights reserved.
http://dx.doi.org/10.1016/j.chaos.2012.06.010

altering the sources and transmission paths. There are two broad categories [11] of vibration control as passive [12] and active control [13–16] technologies.

The most common method used to attenuate vibration from equipment is to mount it on vibration isolator that alters the vibration path. There are many types and configurations of passive vibration isolators [17–19]made of metal springs, synthetic rubber, coiled wire rope and many more. Most of these isolators are designed to operate with a constant linear relationship between the amount of force applied to the isolator and its deflection, which is termed the Hooke's Law of elasticity. Some vibration isolators also operate with a non-linear relationship [20] between the applied force and its displacement. These types of isolators are useful for shock isolation, where a designer might require increasing reaction force as the deflection increases. Reference [18] provides a comprehensive summary of the development of nonlinear passive vibration isolators, that contains over 500 references. A peculiar aspect of non-linear vibration isolators is the potential to use them to obfuscate tonal vibration. In the present study, nonlinear isolators are adopted aiming to provoke complex motion and distort the spectra features of the system.

Generally, active vibration isolation systems use a counter-acting force to reduce the vibration from a source. They are typically used in combination with passive vibration isolation systems, so that if the active system fails, the passive system will still provide some vibration attenuation. There are examples of active vibration isolation systems employed to attenuate vibration from marine engines from reaching the support structure [21]. MTU Friedrichshafen has developed a combined passive and active vibration isolation system for attenuating the vibration from large marine diesel generators [22]. Their results indicate that significant vibration attenuation can be achieved. The development of active vibration control technologies for marine and submarine applications is ongoing in academic and defence research institutions, commercial and defence companies. On the other hand, parameter region for complex motion of the system is quite limited. Due to errors of manufacturing and assembling, it is not friendly feasible to change the component parameters to invoke complex vibration. Consequently, to make the ease of changing system parameter to provoke the system onto complex motion state, we introduce a feedback control to the nonlinear vibration isolation system and obtain a larger parameter region of complex motion.

In the present study, we use both passive and active vibration isolation techniques, that is, introducing a floating raft between the isolated equipment and the base, inserting nonlinear vibration isolators in between, and implementation of a displacement feedback control, aims to suppress the vibration and find the parameter region of the system for complex motion. The present investigation is to study the nonlinear dynamic behaviour of a vibration isolation floating raft system with nonlinear isolators. The approximate analytical solution is obtained by average method [23], which is used to analyze effect of each system parameter on the dynamic vibration behaviour of the system. By numerical integration, periodic motion and complex motions of the system are discussed by tracing the bifurcation diagram,

2. Governing equations

The nonlinear vibration isolation floating raft system can be considered as a 2-DOF mass-spring system [10], as shown in Fig. 1. M_1 and M_2 denote the isolated equipment and the floating raft, respectively. M_1 is supported by a linear damper and a nonlinear spring which possesses both quadric and cubic nonlinearity. The floating raft M_2 is connected with a fixed plane using a linear damper and a cubic nonlinear hardening spring. In addition, there is an actuator between M_1 and M_2, which is utilized to implement feedback control for vibration suppression and complication.

When the origins of coordinates are set at the position where the springs are not compressed, as shown in Fig. 1(a), the equation of the two-DOF nonlinear spring-mass system can be given by

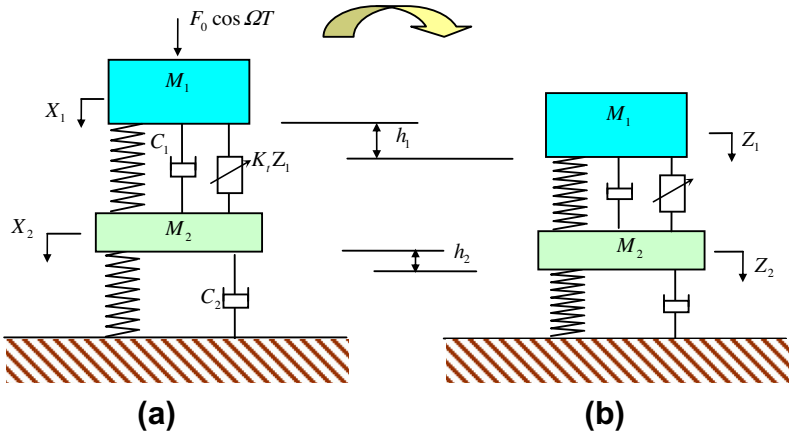

Fig. 1. Vibration isolation floating raft system with (a) the origins of the coordinated located at the uncompressed places and (b) the origins located at the equilibrium places.

$$
\begin{aligned}
&M_1\ddot{X}_1 + C_1(\dot{X}_1 - \dot{X}_2) + K_1(X_1 - X_2) - U_1(X_1 - X_2)^2 \\
&\quad + U_2(X_1 - X_2)^3 = F_0\cos\Omega T + M_1 g \\
&M_2\ddot{X}_2 + C_2\dot{X}_2 + K_2X_2 + U_3X_2^3 = C_1(\dot{X}_1 - \dot{X}_2) + K_1(X_1 - X_2) \\
&\quad - U_1(X_1 - X_2)^2 + U_2(X_1 - X_2)^3 + M_2 g
\end{aligned} \tag{1}
$$

where C_1 is the damping coefficient of the nonlinear vibration isolator; K_1, U_1 and U_2 are the linear, quadric and cubic stiffness coefficients of the nonlinear vibration isolator respectively. C_2 is the damping coefficient of the damper between the floating raft and fixed plane; K_2 and U_3 are the stiffness coefficient of the nonlinear spring between the floating raft and the fixed plane; F_0 and Ω are the amplitude and frequency of harmonic excitation, respectively.

Note that in Fig. 1(a) the origins are not the equilibrium points of this system. After loading the equipment onto the floating raft, i.e. these springs are compressed, the whole system reaches to its equilibrium state as shown in Fig. 1(b). Setting the origins of the new coordinates at the equilibrium state, the relations between the old and new coordinates are:

$$X_1 = Z_1 + h_1, \quad X_2 = Z_2 + h_2 \tag{2}$$

In the equilibrium state, the gravitation terms in Eq. (1) can be eliminated by the following relations:

$$
\begin{aligned}
&K_1H - U_1H^2 + U_2H^3 = M_1 g \\
&K_2h_2 + U_3h_2^3 = M_1 g + M_2 g
\end{aligned} \tag{3}
$$

where $H = h_1 - h_2$.

After the coordinate transformation, the governing equations with feedback control are given by

$$
\begin{aligned}
M_1\ddot{Z}_1 &= -C_1(\dot{Z}_1 - \dot{Z}_2) - (K_1 - 2U_1H + 3U_2H^2)(Z_1 - Z_2) \\
&\quad + (U_1 - 3U_2H)(Z_1 - Z_2)^2 - U_2(Z_1 - Z_2)^3 \\
&\quad + F_0\cos\Omega T + K_tZ_1 \\
M_2\ddot{Z}_2 &= -C_2\dot{Z}_2 - \left(K_2 + 3U_3h_2^2\right)Z_2 - 3U_3h_2Z_2^2 - U_3Z_2^2 \\
&\quad + C_1(\dot{Z}_1 - \dot{Z}_2) + (K_1 - 2U_1H + 3U_2H^2)(Z_1 - Z_2) \\
&\quad - (U_1 - 3U_2H)(Z_1 - Z_2)^2 + U_2(Z_1 - Z_2)^3 - K_tZ_1
\end{aligned} \tag{4}
$$

where K_t is the feedback gain.

Introducing dimensionless parameters

$$
\begin{aligned}
&x_1 = \frac{Z_1}{H}, \quad x_2 = \frac{Z_2}{H}, \quad t = \Omega_0 T, \quad \tau = \Omega_0 T_d, \quad \omega_0 = \frac{\Omega}{\Omega_0}, \\
&\delta_1 = \frac{C_1}{\Omega_0 M_1}, \quad \delta_2 = \frac{C_2}{\Omega_0 M_2}, \quad \eta_1 = \frac{(U_1 - 3U_2H)H}{(K_1 - 2U_1H + 3U_2H^2)}, \\
&\zeta_1 = \frac{U_2H^2}{(K_1 - 2U_1H + 3U_2H^2)}, \quad \eta_2 = \frac{3U_3h_2H}{(K_1 - 2U_1H + 3U_2H^2)}, \\
&\zeta_2 = \frac{U_3H^2}{(K_1 - 2U_1H + 3U_2H^2)}, \quad \mu = \frac{M_1}{M_2}, \\
&f = \frac{F_0}{(K_1 - 2U_1H + 3U_2H^2)H}, \quad k_2 = \frac{K_2}{(K_1 - 2U_1H + 3U_2H^2)}, \\
&k_t = \frac{K_t}{K_1 - 2U_1H + 3U_2H^2}
\end{aligned} \tag{5}
$$

and substituting Eq. (5) into Eq. (4), the first-order form of the dimensionless motion equations are given by

$$
\begin{aligned}
&\ddot{x}_1 + \delta_1(\dot{x}_1 - \dot{x}_2) + (x_1 - x_2) - k_tx_1 \\
&\quad = f\cos\omega_0 t + \eta_1(x_1 - x_2)^2 - \zeta_1(x_1 - x_2)^3 \\
&\ddot{x}_2 + \delta_2\dot{x}_2 + \mu k_2x_2 - \mu\delta_1(\dot{x}_1 - \dot{x}_2) - \mu(x_1 - x_2) + k_t\mu x_1 \\
&\quad = -\mu\eta_1(x_1 - x_2)^2 + \zeta_1\mu(x_1 - x_2)^3 - \eta_2\mu x_2^2 - \zeta_2\mu x_2^3
\end{aligned} \tag{6}
$$

3. Asymptotic solution analyses

To simplify, Eq. (6) can be put in matrix form as

$$\mathbf{M}\ddot{\mathbf{x}} + \mathbf{C}\dot{\mathbf{x}} + \mathbf{K}\mathbf{x} = \mathbf{f} \tag{7}$$

where

$$
\begin{aligned}
&\mathbf{x} = \begin{pmatrix} x_1 \\ x_2 \end{pmatrix}, \quad \mathbf{M} = \begin{pmatrix} 1 & 0 \\ 0 & 1 \end{pmatrix}, \quad \mathbf{C} = \begin{pmatrix} \delta_1 & -\delta_1 \\ -\mu\delta_1 & \delta_2 + \mu\delta_1 \end{pmatrix}, \\
&\mathbf{K} = \begin{pmatrix} 1 - k_t & -1 \\ (k_t - 1)\mu & \mu(k_2 + 1) \end{pmatrix} \\
&\mathbf{f} = \begin{pmatrix} f\cos\omega_0 t + \eta_1(x_1 - x_2)^2 - \zeta_1(x_1 - x_2)^3 \\ -\mu\eta_1(x_1 - x_2)^2 + \zeta_1\mu(x_1 - x_2)^3 - \eta_2\mu x_2^2 - \zeta_2\mu x_2^3 \end{pmatrix}, \\
&\phi = \omega_0 t
\end{aligned} \tag{8}
$$

Applying the method of averaging, the steady state responses are assumed as

$$
\begin{aligned}
&\mathbf{x}(t) = \mathbf{u}(t)\cos\phi + \mathbf{v}(t)\sin\phi \\
&\dot{\mathbf{x}}(t) = -\mathbf{u}(t)\sin\phi + \mathbf{v}(t)\cos\phi
\end{aligned} \tag{9}
$$

where

$$\mathbf{u}(t) = \begin{pmatrix} u_1(t) \\ u_2(t) \end{pmatrix}, \quad \mathbf{v}(t) = \begin{pmatrix} v_1(t) \\ v_2(t) \end{pmatrix} \tag{10}$$

which are assumed to be slow functions about the time t.

Differentiating the first formula of Eq. (9) with respect to the time t, we obtain

$$\dot{\mathbf{x}}(t) = \dot{\mathbf{u}}(t)\cos\phi - \mathbf{u}(t)\omega_0\sin\phi + \dot{\mathbf{v}}(t)\sin\phi + \mathbf{v}(t)\omega_0\cos\phi \tag{11}$$

Substituting the second formula in Eq. (9) into Eq. (11), the resulting equation is

$$\dot{\mathbf{u}}(t)\cos\phi + \dot{\mathbf{v}}(t)\sin\phi = 0 \tag{12}$$

Also differentiating the second formula of Eq. (9), we obtain

$$\ddot{\mathbf{x}}(t) = -\dot{\mathbf{u}}(t)\omega_0\sin\phi - \mathbf{u}(t)\omega_0^2\cos\phi + \dot{\mathbf{v}}(t)\omega_0\cos\phi - \mathbf{v}(t)\omega_0^2\sin\phi \tag{13}$$

Substituting the expressions about $\ddot{\mathbf{x}}(t), \dot{\mathbf{x}}(t)$ and $\mathbf{x}(t)$ into Eq. (7), the following equation is found:

$$
\begin{aligned}
&(\mathbf{M}\dot{\mathbf{v}}\omega_0 - \mathbf{M}\mathbf{u}\omega_0^2 + \mathbf{C}\mathbf{v}\omega_0 + \mathbf{K}\mathbf{u})\cos\phi \\
&\quad - (\mathbf{M}\dot{\mathbf{u}}\omega_0 + \mathbf{M}\mathbf{v}\omega_0^2 + \mathbf{C}\mathbf{u}\omega_0 - \mathbf{K}\mathbf{v})\sin\phi = \mathbf{f}(\mathbf{u}, \mathbf{v}, t)
\end{aligned} \tag{14}
$$

Then, Eq. (12) is multiplied by $\mathbf{M}\omega_1\cos\phi$; Eq. (14) is multiplied by $-\sin\phi$ and the two equations are added. The

resulting equation is then integrated from 0 to 2π by assuming that $\mathbf{u}$ and $\mathbf{v}$ remain constant. The final result is

$$\mathbf{M}\dot{\mathbf{u}}\omega_0 = \frac{1}{2}(\mathbf{K} - \mathbf{M}\omega_0^2)\mathbf{v} - \frac{1}{2}\mathbf{C}\mathbf{u}\omega_0 + \frac{1}{2}\begin{pmatrix} q_{11} \\ -\mu q_{12} \end{pmatrix} \tag{15}$$

Similarly, Eq. (12) is multiplied by $\mathbf{M}\omega_1\sin\phi$; Eq. (14) is multiplied by $\cos\phi$ and the two equations are added. Then, integrating the resulting equation from 0 to 2π; we obtain

$$\mathbf{M}\dot{\mathbf{v}}\omega_0 = -\frac{1}{2}(\mathbf{K} - \mathbf{M}\omega_0^2)\mathbf{u} - \frac{1}{2}\mathbf{C}\mathbf{v}\omega_0 + \frac{1}{2}\begin{pmatrix} -q_{21} \\ \mu q_{22} \end{pmatrix} + \frac{1}{2}\begin{pmatrix} f_0 \\ 0 \end{pmatrix} \tag{16}$$

where

$$\begin{aligned} q_{11} &= \frac{3}{4}[(u_1-u_2)^2 + (v_1-v_2)^2](v_1-v_2)\zeta_1 \\ q_{12} &= \frac{3}{4}\{[(u_1-u_2)^2 + (v_1-v_2)^2](v_1-v_2)\zeta_1 - v_2(u_2+v_2)^2\zeta_2\} \\ q_{21} &= \frac{3}{4}[(u_1-u_2)^2 + (v_1-v_2)^2](u_1-u_2)\zeta_1 \\ q_{22} &= \frac{3}{4}\{[(u_1-u_2)^2 + (v_1-v_2)^2](u_1-u_2)\zeta_1 + v_2(u_2+v_2)^2\zeta_2\} \end{aligned} \tag{17}$$

Eqs. (15) and (16) represent a set of first order, ordinary differential equations. For the periodic steady state vibration, the conditions are given as

$$\dot{\mathbf{u}} = \dot{\mathbf{v}} = 0 \tag{18}$$

Substituting conditions (18) into Eqs. (15) and (16), a set of four coupled non-linear algebraic equations for u_1, v_1, u_2 and v_2 is obtained:

$$\begin{aligned} &u_1\delta_1\omega_0 - u_2\delta_1\omega_0 + v_1(\omega_0^2 + k_t - 1) + v_2 - q_{11} = 0 \\ &u_1\delta_1\mu\omega_0 - u_2(\delta_1+\delta_2)\mu\omega_0 + v_1\mu(k_t-1) \\ &\quad + v_2(\mu - \omega_0^2 + k_2\mu) - \mu q_{12} = 0 \\ &u_1(\omega_0^2 + k_t - 1) + u_2 - v_1\delta_1\omega_0 + v_2\delta_1\omega_0 - q_{21} + f_0 = 0 \\ &u_1\mu(1-k_t) + u_2(\omega_0^2 - \mu - k_2\mu) + v_1\delta_1\mu\omega_0 \\ &\quad - v_2(\delta_1+\delta_2)\mu\omega_0 + \mu q_{22} = 0 \end{aligned} \tag{19}$$

The response amplitudes of the isolated equipment and the floating raft are denoted as r_1 and r_2, respectively, namely

$$r_1 = \sqrt{u_1^2 + v_1^2}, \quad r_2 = \sqrt{u_2^2 + v_2^2} \tag{20}$$

4. Numerical simulations

The following numerical simulations demonstrate and verify the effectiveness of the approach and derived analytical results. The fourth-order Runge–Kutta method is used to integrate the differential equations for numerical results with Matlab. The dimensionless parameters of the nonlinear VIS are set as $\delta_1 = 0.02$, $\delta_2 = 0.02$, $\zeta_1 = 0.5$, $\zeta_2 = 0.5$, $\mu = 0.5$, $k_2 = 2$, $f = 0.5$, $k_t = 0$, if without other specification. Since we are most interested in the vibration amplitude and features of the floating raft M_2, which is connected to the base, in the follow figures r_2 denotes the vibration amplitude of floating raft M_2 and ω_0 is the dimensionless excitation frequency.

Fig. 2 shows the comparison between the approximate solution in Eq. (20) obtained by the average method and numerical results from Eq. (6) by Matlab for the linear ($\zeta_1 = 0$, $\zeta_2 = 0$) and nonlinear system ($\zeta_1 = 0.5$, $\zeta_2 = 0.5$). The system parameters are set as $\delta_1 = 0.02$, $\delta_2 = 0.02$, $\eta_1 = 0$, $\eta_2 = 0$, $\mu = 0.5$, $k_2 = 2$, $f = 0.5$, $k_t = 0$ and the initial condition for numerical solution is (0,0,0,0). From Fig. 2(a), it can be seen that the two sets of results agree with each other very well. This is because when the system is linear, the system takes on periodic vibration under the harmonic excitation. It also shows that the natural frequencies of the system is 0.75 and 1.4. However, in Fig. 2(b), we can see a small discrepancy at $\omega_0 = 0.25$ and the overall tendency of the two sets are the same. As the initial condition is at the original equilibrium, so the numerical results show the system vibrates with amplitude at the low resonance branch and two jumping up phenomenon can be observed. We also study a case in Fig. 3 with frequency $\omega_0 = 0.25$, where the two results present a difference.

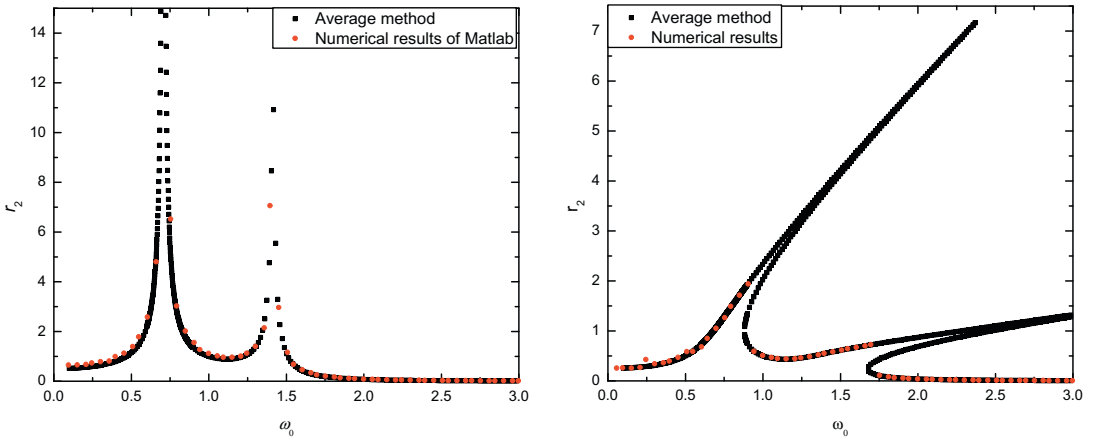

(a) Linear system with $\zeta_1 = 0, \zeta_2 = 0$ (b) Nonlinear system with $\zeta_1 = 0.5, \zeta_2 = 0.5$

Fig. 2. Comparison of the results from approximate solution and numerical solution.

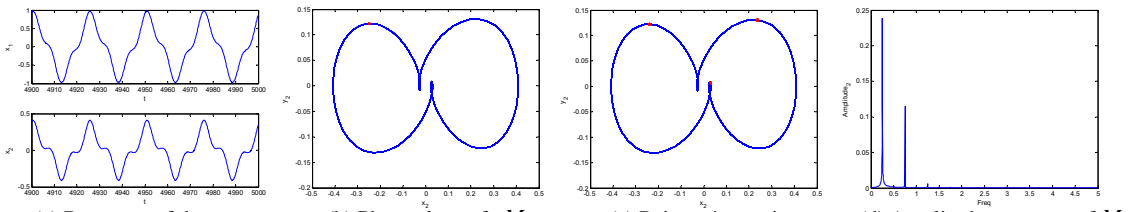

(a) Response of the system (b) Phase plane of M_2 (c) Poincaré mapping (d) Amplitude spectrum of M_2

Fig. 3. Validation of discrepancy in Fig. 2 with $\omega_0 = 0.25$.

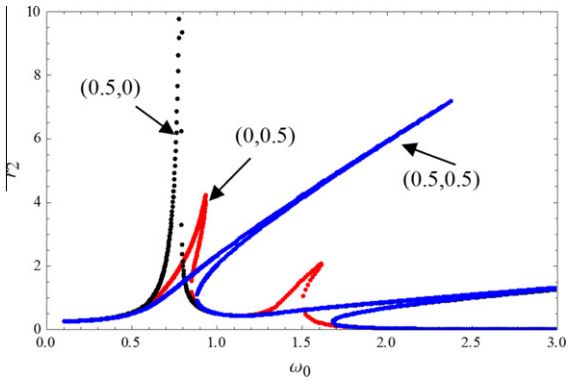

Fig. 4. Effect of nonlinear parameters (ζ_1, ζ_2) on the amplitude–frequency curves of floating raft.

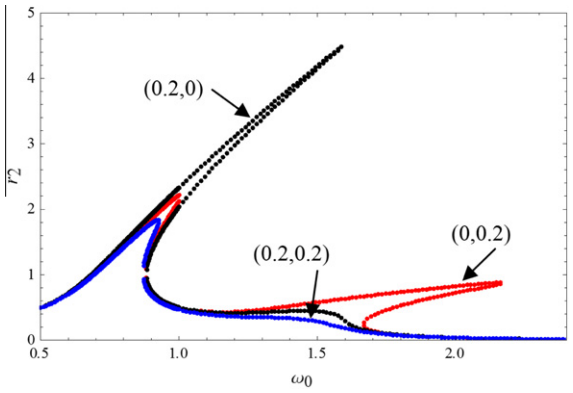

Fig. 5. Effect of damping parameters (δ_1, δ_2) on the amplitude–frequency curves of floating raft.

From Fig. 3, it can be noted that the system takes on three times periodic vibration. In Fig. 3(a), the time history responses of the system show the vibration amplitude x_2 is 0.4, as stated in Fig. 2(b), which is different from the analytical solution with amplitude 0.3. Also, the vibration amplitude of x_2 is less than half of x_1, so this means introduction of floating raft to the vibration isolation system can reduce the vibration transmitted to the base. Fig. 3(b) shows the phase plane and Poincaré mapping of the system. The phase plane presents three circles rather than a simple closed curve for periodic vibration. Obviously, Fig. 3(d) shows the system has another line spectra at $3\omega_0$, besides the one at the excitation frequency $\omega_0 = 0.25$, which is called 3-order superharmonic vibration. But, we assume the analytical solution only with the excitation frequency, not taking into account of the subharmonic and superharmonic caused by nonlinearity, so this is where the discrepancy comes from. On the other hand, since the Poincaré section maps at every period of the excitation frequency, that is, $2\pi/\omega_0$, it cannot show superharmonic vibration. When set the Poincaré mapping interval at $2\pi/(3\omega_0)$, 3 points are presented in Fig. 3(c). Anyway, we can remark that the analytical solution attained in the last section can describe the system under one periodic vibration correctly. Thus, in the follow, we use the analytical solution to conduct qualitative analysis for the nonlinear vibration isolation floating raft system.

Fig. 4 shows the amplitude–frequency curves of the nonlinear vibration isolation system with different nonlinear parameters, where $\zeta_1 = 0$ or $\zeta_2 = 0$ denotes the upper isolator or the lower isolator is linear. Other system parameters are set as $\delta_1 = 0.02$, $\delta_2 = 0.02$, $\mu = 0.5$, $k_2 = 2$, $f = 0.5$, $k_t = 0$.Comparing the three set of curves, it can be noted that as long as there is nonlinearity in the system, the second resonance is bent, while there is no jumping region at the adjacent region of the first resonance peak for some nonlinear parameters combination. Besides, increasing the nonlinearity of the upper isolator, the second resonance peak have a lower amplitude and increase of the nonlinear parameter of the lower isolator can reduce the amplitude of the first resonance peak. Comparing the three curves with ω_0 ranges from $(0, 0.7)$ along with Fig. 2(a), the curves with $(\zeta_1, \zeta_2) = (0.5, 0.5)$ has the minimum vibration amplitude. This means nonlinearity can attenuate the vibration amplitude significantly. Moreover, appropriate combination of nonlinear coefficient of the isolators can achieve a more desirable effect. The amplitude–frequency curve with $(0, 0.5)$ has small jumping region in the neighbourhood of the two resonance peaks, while the curve with $(0.5, 0)$ has a jumping region from $\omega_0 = 1.67$ to 3, and the amplitude-frequency curve with $(0.5, 0.5)$ has a far larger jumping region starting from 0.9. As we known, among the jumping region the system has more than one solution, especially unstable solution. Therefore with frequency the jumping region it is easier to complicate the system to obtain double period, quasi-period or chaotic motion.

Effect of damping parameters on the amplitude-frequency curves are presented in Fig. 5, with δ_1 and δ_2 being the damping coefficients of the upper and lower isolator. The system parameters are set as $\zeta_1 = 0.5$, $\zeta_2 = 0.5$, $\mu = 0.5$, $k_2 = 2, f = 0.5$, $k_t = 0$. From the figure, it can be observed that

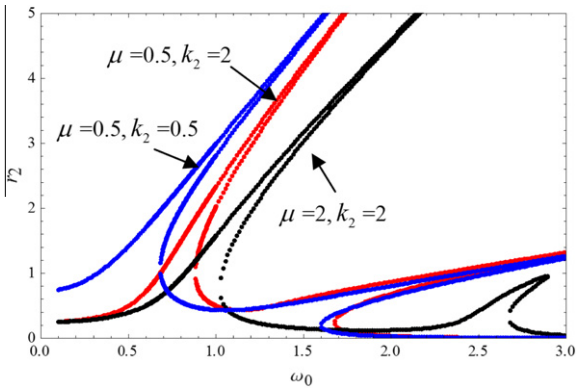

Fig. 6. Effect of stiffness and mass ratio on the amplitude–frequency curves of floating raft.

damping of the upper isolator can reduce the amplitude of the second resonance greatly and the lower isolator damping can suppress the vibration amplitude of the floating raft better when the frequency is around the first resonance frequency. When ω_0 locates at (0,0.9), damping of the lower isolator has a better vibration attenuation than the upper one. With combination of the two damp pot, the vibration amplitude of the floating raft can be further suppressed. To achieve vibration attenuation at different frequency region, different combination of damping of the isolators can be designed.

Fig. 6 presents effect of different stiffness of the lower isolator and the mass ratio of $\mu(M_1/M_2)$ on the amplitude–frequency curves of the floating raft in the nonlinear vibration isolation system. The system parameters are set as $\delta_1 = 0.02$, $\delta_2 = 0.02$, $\zeta_1 = 0.5$, $\zeta_2 = 0.5$, $f = 0.5$, $k_t = 0$. When $\mu = 2 > 1$, that is, $M_1 > M_2$, amplitude of the floating raft become smaller and the second resonance peak is suppressed dramatically. The two resonance frequency increases. Hence, by design of the mass ratio, we can put the resonance region into higher frequency where the vibration attenuation can be easier achieved. When $k_2 = 0.5 < 1$, i.e. the lower isolator is softer than the upper one, amplitude of the floating raft with frequency among the first jumping region is larger, while that within the second jumping region is smaller. When ω_0 is set in the region (0,0.65), the curve with $(\mu = 2, k_2 = 2)$ has the lowest vibration amplitude. It means that to attenuate vibration at lower frequency, $M_1 > M_2$ and harder isolator in the lower layer yield a better effect.

Fig. 7 shows the effect of feedback control gain on the dynamic behaviour of the system. The system parameters are set as $\delta_1 = 0.02$, $\delta_2 = 0.02$, $\zeta_1 = 0.5$, $\zeta_2 = 0.5$, $\mu = 0.5$, $k_2 = 2$, $f = 0.5$. Increase of control gain does not change the maximum of the peaks much, but it bring the resonance frequency forward with positive control gains. This is because introduction of positive control is equivalent to reduce the stiffness of the upper isolator. Hence, the resonance frequencies are reduced. By comparing the four sets of curves among (0,0.75), it can be noted that the curve with $k_t = -0.4$ has the minimum vibration amplitude. Hence we can remark that, introducing of negative feedback control can attenuate the vibration of the floating raft at lower frequency. In addition, negative feedback control can also bring the resonance frequency backwards to higher frequency which is more desirable for vibration attenuation.

In what follows, we conduct numerical simulation of Eq. (6) to understand more complicated nonlinear behaviour of the system. Since, adjusting the exciting frequency and control gain is more feasible than altering the other system component parameters, only the bifurcation diagrams with ω_0 and k_t are investigated in the present study. In Fig. 8, system parameters are $\delta_1 = 0.01$, $\delta_2 = 0.01$, $\zeta_1 = 0.5$, $\zeta_2 = 0.5$, $\mu = 0.5$, $k_2 = 2$, $f = 1$, $k_t = 0$. Fig. 8 shows the bifurcation diagram of the floating raft by using exciting frequency ω_0 as bifurcation parameter . It can be seen from the figure that there are three discontinuity phenomenon located as $\omega_0 = 0.648$, 1.036 and 1.904, respectively, the later two of which correspond to the jumping up frequency in the amplitude–frequency curves. Besides, motion status of the system changes with increase of exciting frequency. When ω_0 among the range of (0.5,0.648), the system takes period 1 vibration. When ω_0 falls into (0.648,0.71), the floating raft exhibits superharmonic vibration (as shown

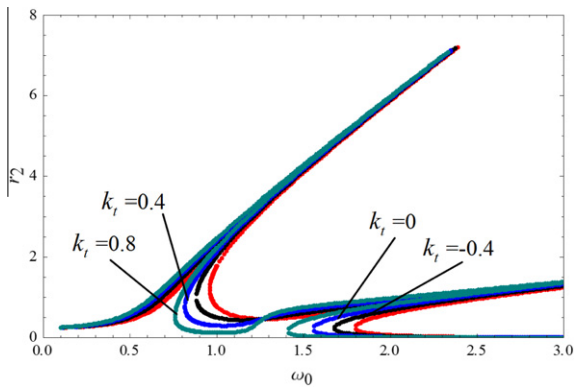

Fig. 7. Effect of control gain k_t on the amplitude–frequency curves of floating raft.

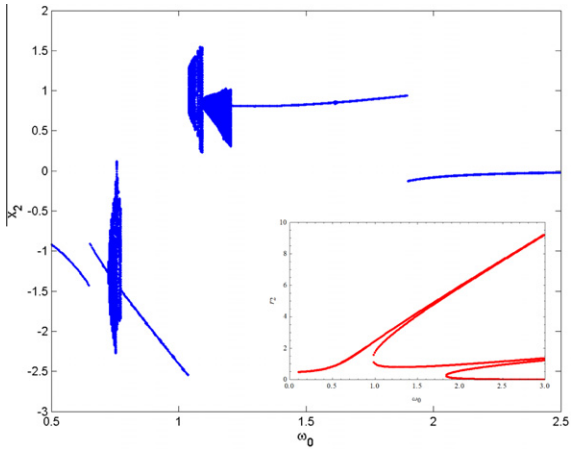

Fig. 8. Bifurcation diagram of the floating raft versus frequency.

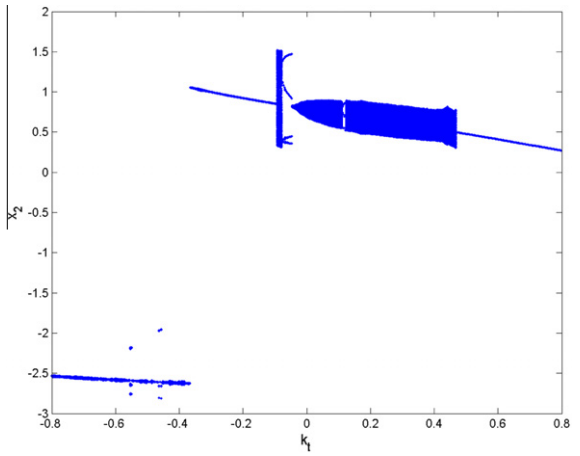

Fig. 9. Bifurcation diagram of the floating raft versus control gain ($\omega_0 = 1.1$).

in Fig. 10(b)). With ω_0 at (0.71,0.77), the floating raft vibrates in the term of complex motion. From $\omega_0 = 0.77$ to 1.048, the system takes on period 1 motion. Among the range of (1.048,1.116) and (1.116,1.22), the floating raft enters into complex motion. When $\omega_0 > 1.22$, the system takes on periodic vibration. The corresponding phase plane and Poincaré mapping are shown in Fig. 10. It can be concluded that by changing the exciting frequency, motion features of the vibration system can be altered.

Fig. 9 presents the bifurcation diagram of the floating raft with control gain k_t as bifurcation parameter and system parameters are $\delta_1 = 0.01$, $\delta_2 = 0.01$, $\zeta_1 = 0.5$, $\zeta_2 = 0.5$, $\mu = 0.5$, $k_2 = 2$, $f = 1$, $\omega_0 = 1.1$. The system exhibits periodic, double periodic and complex motions for different control gain. When the control gain falls into $(-0.8, -0.096)$, the system enters into periodic motion. While k_t is among the range of $(-0.096, -0.08)$, the floating raft takes on complex motion. With k_t at $(-0.08, -0.048)$, the system takes on period 4 motion. From $k_t = -0.0384$ to 0.48, complex motion occurs to the floating raft, except that there is a small region around $k_t = 0.112$ where the floating raft takes on period 3 motion. When $k_t > 0.48$, the system exhibits period 1 motion. The corresponding phase plane and Poincaré mapping are shown in Fig. 11. We can remark that complex motion can be obtained by adjusting the control gain.

In Fig. 10, the phase plane and Poincaré mapping for the floating raft of the nonlinear vibration isolation system are shown for different exciting frequencies. At $\omega_0 = 0.5$ Fig. 10(a), $\omega_0 = 0.8$ (Fig. 10(e)), $\omega_0 = 1.08$ (Fig. 10(h)) and $\omega_0 = 1.3$ (Fig. 10(j)), there occurs a closed curve, which means the system takes on periodic 1 vibration. At $\omega_0 = 0.7$ (Fig. 10(b)), there are three circles in the closed curves and one mapping point, showing that the system is on superharmonic vibration (similar to the case in Fig. 3 and the spectrum is not presented here). At $\omega_0 = 0.75$, 1.05 and 1.1, corresponding to Fig. 10(c), (f) and (i), which demonstrate complex phase plane and closed curve for Poincaré mapping, the system exhibits quasi-periodic motions. While at $\omega_0 = 0.764$ (Fig. 10(d)) and $\omega_0 = 1.072$ (Fig. 10(g)), the system enters into doubling periodic motion. Comparing the figures in Fig. 10, we remark that motion status of the system is much sensitive to the exciting frequency.

Fig. 11 presents the phase plane and Poincaré mapping for the floating raft of the nonlinear vibration isolation system, which verifies the bifurcation diagram in Fig. 9. From the numerical simulation case study in Fig. 11, it can be noted that when $k_t = -0.6$ (Fig. 11(a)), $k_t = -0.5$ (Fig. 11(c)) and $k_t = 0.5$ (Fig. 11(g)), the system takes on period 1 vibration. While in Fig. 11(f), i.e. $k_t = -0.048$, the system takes on period 4 vibration. In Fig. 11 (b), (d) and (h), the system exhibits period 3 vibration. In cases (e), (g) and (i), the quasi-periodic motion occurs to the system. From Fig. 11(a) to Fig. 11(i), it can be concluded that the feedback control has a great effect on the dynamic behaviour of the system. We can implement a feedback control to a system to achieve some intended goals. In addition, it can be noted that the vibration amplitude of the floating raft varies with change of control gain. In Fig. 11(j) $k_t = 0.5$, the floating raft has amplitude of less than 0.6, which is the minimum among all these ten cases.

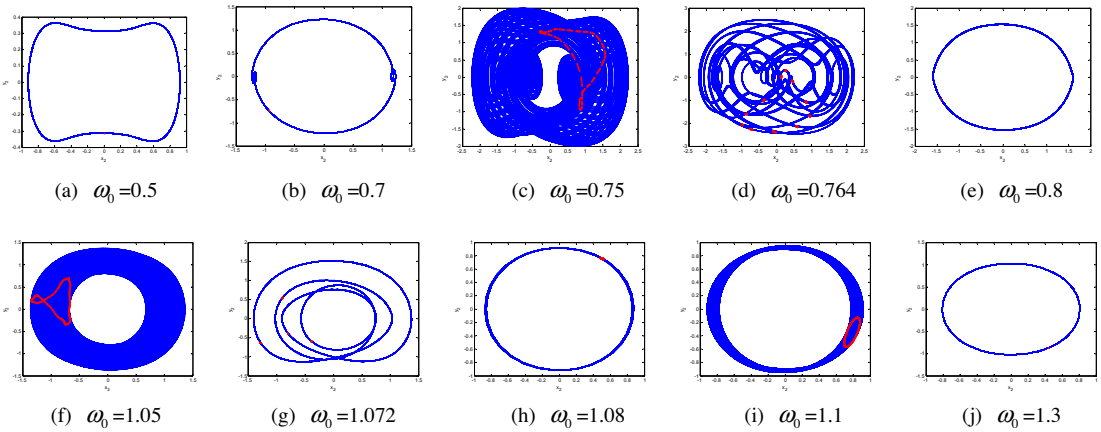

Fig. 10. Phase plane of the floating raft for different exciting frequencies.

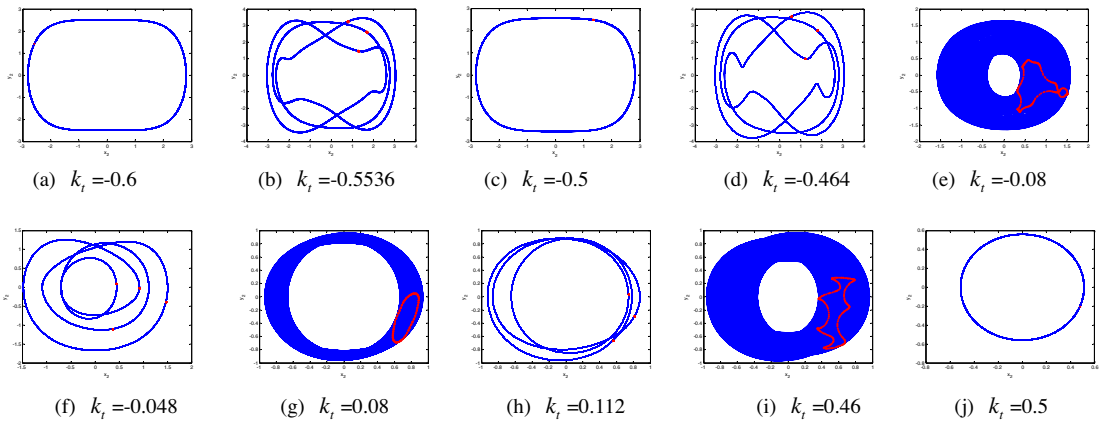

Fig. 11. Phase plane of the floating raft for different control gains.

5. Conclusions

In the present study, we introduce a floating raft between the isolated equipment and the base, and implement a displacement feedback control, in order to suppress the vibration and find the parameter region of the system for complex motion. The dynamic behaviour of the vibration isolation floating raft system is studied by analytical solution from average method. Results show the effect of reduction the vibration amplitude can be obtained by properly adjusting the values of the damping parameters, nonlinear spring stiffness, mass ratio and the range of exciting frequency. Moreover, the displacement feedback control gain plays a great role on the nonlinear dynamic behaviour of the system. By adjusting the control gain or exciting frequency, vibration features of the nonlinear vibration isolation system can be altered and complex motion can be obtained.

Acknowledgements

This research work was supported by the research grant of Chaos-Floating raft Isolation Technology (799215116), the National Natural Science Foundation of China (11072075, 11072076, 11102062), and the research grant (71075004) from the State Key Lab of Advanced Design and Manufacturing for Vehicle Body.

References

[1] Howard CQ. A new cost function algorithm for adaptive-passive vibration and acoustic resonators. Proc Acoust 2011:2–4.
[2] Choi SB, Sohn JW, Choi SM, Nguyen VQ, Moon SJ. A piezostack-based active mount for broadband frequency vibration control: experimental validation. Smart Mater Struct 2009;18:097001.
[3] Dylejko PG, Kessissoglou NJ, Tso Y, Norwood CJ. Optimisation of a resonance changer to minimise the vibration transmission in marine vessels. J Sound Vib 2007;300:101–16.
[4] Caresta M, Kessissoglou NJ. Reduction of hull-radiated noise using vibroacoustic optimization of the propulsion system. J Ship Res; 55. p. 149–62.
[5] Howard CQ, Craig RA. Adaptive-passive quarter-wave tube resonator silencer. In: Proceedings of Acoustics 2011: annual conference of the Australian Acoustical Society 2011.
[6] Liu S, Zhu S, Yu X, Lou J. Study on chaotic parameter range of nonlinear vibration isolation system. In: Proceedings of the 2004 international symposium on safety science and technology. Shanghai, China; 2004. p. 2064–8.
[7] Lou JJ, Zhu SJ, He L, Yu X. Application of chaos method to line spectra reduction. J Sound Vib 2005;286:645–52.
[8] Liu S, Yu X, Zhu S. Study on the chaos anti-control technology in nonlinear vibration isolation system. J Sound Vib 2008;310:855–64.
[9] Lou JJ, Zhu SJ, He L, He QW. Experimental chaos in nonlinear vibration isolation system. Chaos Solitons Fract 2009;40:1367–75.
[10] Yu X, Zhu S, Liu S. A new method for line spectra reduction similar to generalized synchronization of chaos. J Sound Vib 2007;306:835–48.
[11] Howard CQ. Recent developments in submarine vibration isolation and noise control. In: Conference 2011 presentations & proceedings on USB.
[12] Rivin EI. Passive vibration isolation: American Society of Mechanical; 2003.
[13] Pan X, Tso Y, Juniper R. Active control of radiated pressure of a submarine hull. J Sound Vib 2008;311:224–42.
[14] Pan X, Tso Y, Juniper R. Active control of low-frequency hull-radiated noise. J Sound Vib 2008;313:29–45.
[15] Sievers LA, von Flotow AH. Linear control design for active vibration isolation of narrow band disturbances. IEEE 1988;2:1032–7.
[16] Sas P, Bao C, Augusztinovicz F, Desmet W. Active control of sound transmission through a double panel partition. J Sound Vib 1995;180:609–26.
[17] Rivin EI. Passive vibration isolation. Appl Mech Rev 2004;57:B31.
[18] Ibrahim RA. Recent advances in nonlinear passive vibration isolators. J Sound Vib 2008;314:371–452.
[19] Lagoudas DC, Khan MM, Mayes JJ, Henderson BK. Pseudoelastic SMA spring elements for passive vibration isolation: Part II simulations and experimental correlations. J Intell Mater Syst Struct 2004;15:443–70.
[20] Kovacic I, Brennan MJ, Waters TP. A study of a nonlinear vibration isolator with a quasi-zero stiffness characteristic. J Sound Vib 2008;315:700–11.
[21] Howard CQ. Technologies for the Management of the Acoustic Signature of a Submarine. In: Proceedings of the Submarine Institute of Australia 2010: SIA 5th Biennial Conference 2010.
[22] Drathen AV. Propulsion system solutions for present and future naval vessels. Pacific. Sydney, Australia 2010.
[23] Zhu SJ, Zheng YF, Fu YM. Analysis of non-linear dynamics of a two-degree-of-freedom vibration system with non-linear damping and non-linear spring. J Sound Vib 2004;271:15–24.